ENVIRONMENTAL STUDIES

Isoprene photo-oxidation products quantify the effect of pollution on hydroxyl radicals over Amazonia

Yingjun Liu,[1]* Roger Seco,[2] Saewung Kim,[2] Alex B. Guenther,[2] Allen H. Goldstein,[3] Frank N. Keutsch,[1,4] Stephen R. Springston,[5] Thomas B. Watson,[5] Paulo Artaxo,[6] Rodrigo A. F. Souza,[7] Karena A. McKinney,[1†‡] Scot T. Martin[1,8‡]

Nitrogen oxides (NO_x) emitted from human activities are believed to regulate the atmospheric oxidation capacity of the troposphere. However, observational evidence is limited for the low-to-median NO_x concentrations prevalent outside of polluted regions. Directly measuring oxidation capacity, represented primarily by hydroxyl radicals (OH), is challenging, and the span in NO_x concentrations at a single observation site is often not wide. Concentrations of isoprene and its photo-oxidation products were used to infer the equivalent noontime OH concentrations. The fetch at an observation site in central Amazonia experienced varied contributions from background regional air, urban pollution, and biomass burning. The afternoon concentrations of reactive nitrogen oxides (NO_y), indicative of NO_x exposure during the preceding few hours, spanned from 0.3 to 3.5 parts per billion. Accompanying the increase of NO_y concentration, the inferred equivalent noontime OH concentrations increased by at least 250% from 0.6×10^6 to 1.6×10^6 cm^{-3}. The conclusion is that, compared to background conditions of low NO_x concentrations over the Amazon forest, pollution increased NO_x concentrations and amplified OH concentrations, indicating the susceptibility of the atmospheric oxidation capacity over the forest to anthropogenic influence and reinforcing the important role of NO_x in sustaining OH concentrations.

INTRODUCTION

Earth's atmosphere is an oxidizing medium that drives organic molecules toward carbon dioxide, and oxidation by hydroxyl radicals (OH) initiates most of these reactions (*1*, *2*). Oxidation by OH radicals also leads to the production of many secondary pollutants that affect human health and climate, such as organic particulate matter and ozone. In relation to OH concentrations, the NO_x family, defined as including nitric oxide (NO) and nitrogen dioxide (NO_2), has two roles (*2*). The chemistry is illustrated in Fig. 1A. On the one hand, NO reacts with hydroperoxyl radicals (HO_2) and organic peroxyl radicals (RO_2) to produce OH catalytically in the presence of sunlight, thereby enhancing OH concentrations. On the other hand, at higher NO_x concentrations, the direct reaction of NO_2 with OH to produce nitric acid (HNO_3) becomes dominant, and NO_x serves as an OH sink. Hydroxyl radical concentrations thus increase as NO_x concentrations increase below a threshold NO_x concentration, and they decrease as NO_x concentrations increase above this threshold. The net result is that OH concentrations follow a bell curve with respect to NO_x concentrations, as illustrated in Fig. 1B (*2*, *3*).

The applicability of this classical understanding of OH-NO_x chemistry, as represented by the bell curve, to atmospheric conditions is under challenge based on field measurements of OH concentrations in regions where volatile organic compounds (VOCs) are abundant. A meta-study examined the dependence of OH concentrations across a broad range of NO_x conditions (*4*). The observations ranged from tropical forests in South America and Southeast Asia (*5*, *6*) to deciduous forest in the United States and rural area in China (*7*–*9*) and to polluted metropolitan regions of New York City, Beijing, Tokyo, and Mexico

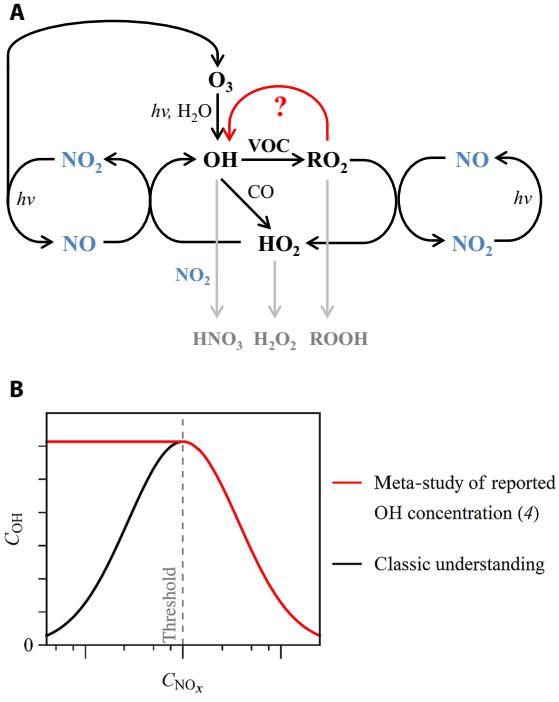

Fig. 1. Illustration of the relationship of OH and NO_x. (**A**) Chemical cycles connecting OH production and loss to NO_x and VOC species. (**B**) Dependence of OH concentration on NO_x concentration. The classical dependence of the bell curve in black can be compared to the absence of a dependence (that is, the red horizontal line) below a threshold NO_x concentration, as suggested by the meta-study of Rohrer *et al.* (*4*).

[1]School of Engineering and Applied Sciences, Harvard University, Cambridge, MA 02138, USA. [2]Department of Earth System Science, University of California, Irvine, Irvine CA 92697, USA. [3]Department of Environmental Science, Policy and Management, University of California, Berkeley, Berkeley, CA 94720, USA. [4]Department of Chemistry and Chemical Biology, Harvard University, Cambridge, MA 02138, USA. [5]Department of Environmental and Climate Sciences, Brookhaven National Laboratory, Upton, NY 11973, USA. [6]Department of Applied Physics, University of São Paulo, São Paulo 05508, Brazil. [7]Department of Meteorology, Amazonas State University, Manaus, Amazonas 69050, Brazil. [8]Department of Earth and Planetary Sciences, Harvard University, Cambridge, MA 02138, USA.
*Present address: Department of Environmental Science, Policy and Management, University of California, Berkeley, Berkeley, CA 94720, USA.
†Present address: Department of Chemistry, Colby College, Waterville, ME 04901, USA.
‡Corresponding author. Email: scot_martin@harvard.edu (S.T.M.); kamckinney@seas.harvard.edu (K.A.M.)

City (*10*–*13*). Above a threshold NO_x concentration, OH concentrations decreased with increasing NO_x concentration, as expected. However, below the threshold NO_x concentration, reported OH concentrations in many regions were unexpectedly high, and collectively, they appeared to be independent of NO_x concentration, as illustrated by the horizontal line in Fig. 1B.

Possible mechanisms for maintaining elevated OH concentrations under atmospheric conditions with below-threshold NO_x concentrations have been considered (*7*, *14*–*16*). In regions where VOCs are abundant, especially over and downwind of forests, the major fate of OH is reaction with biogenic VOCs to produce RO_2. Possible reactions of RO_2 radicals to regenerate OH and thereby maintain OH concentrations have been suggested, especially for forested regions dominated by isoprene emissions, such as OH production from the reaction of HO_2 with isoprene-derived RO_2 radicals (ISOPOO) (*14*, *17*), as well as OH release following ISOPOO isomerization (*16*, *18*). Even so, these mechanisms appear insufficient to quantitatively explain the reported high OH concentrations at low NO_x concentrations (*14*, *17*, *18*). Alternatively, the accuracy of reports of high OH concentrations is uncertain because of the possibility of interferences in the underlying measurement technique of laser-induced fluorescence (LIF) (*9*, *19*, *20*). For instance, Mao *et al.* (*9*) attributed 40 to 60% of the nominal OH signal observed in a California forest to interferences. After correction, the data fell on the bell curve, instead of on the horizontal line of Fig. 1B (*4*). To date, there is no consensus on whether similar interferences may have occurred in the other measurements included in the meta-study. The LIF instruments are custom-built in variable configurations by different research groups. Another uncertainty related to the meta-study is that the span in NO_x concentration of each underlying study was usually not wide, so no individual study closely tested the response of OH concentration to NO_x concentration across a broad range. Instead, the analysis in the meta-study was based on normalization of observations across multiple sites, different instruments, and differing atmospheric conditions. In short, possible new mechanisms for OH production and recycling under atmospheric conditions and possible artifacts in the underlying data sets all remain to be reconciled.

Herein, a complementary approach based on isoprene photooxidation products is presented for mapping the dependence of OH concentration on NO_x concentration for atmospheric conditions over an isoprene-dominated forested environment. Precedent approaches for estimating OH concentrations include the use of a range of OH-reacting trace species, as well as OH reaction products and their ratios (*3*, *21*–*24*). Isoprene is the dominant VOC emitted to the atmosphere from many forests (*25*), and reaction with OH is its primary loss pathway (*26*). As OH concentration increases, the concentration C_{ISOP} of isoprene decreases, and the sum concentration C_{PROD} of its oxidation products increases, provided that other factors, such as reaction time, ozone concentration, and isoprene emission rates, are unchanged. The presentation herein develops an analysis to use the afternoon parent-to-product concentration ratio C_{ISOP}/C_{PROD} to infer equivalent noontime OH concentration within an air mass during the preceding daylight hours. The analysis must account for several factors, in addition to OH concentration, that influence C_{ISOP}/C_{PROD}.

Data sets were recorded at a single site in the *Observations and Modeling of the Green Ocean Amazon* (GoAmazon2014/5) Experiment in central Amazonia during the wet and dry seasons of 2014 (*27*). At different times, the sampling site received mixtures to various degrees of unpolluted regional background air, air influenced by regional fires (especially in the dry season), or air that had passed over the nearby city of Manaus, an urban region of 2 million inhabitants and a strong regional source of NO_x. The site was 4 to 6 hours downwind from Manaus for the typical prevailing easterlies associated with trade winds (*27*, *28*). As a result, the GoAmazon2014/5 data sets spanned a great breadth of upwind NO_x chemistry at a single observation site (*29*). The range in measured isoprene concentrations was similar to that of the forested sites of the meta-study (*4*). The GoAmazon2014/5 data sets were used in the analysis herein to strongly test for a bell curve versus a horizontal line in the response of OH concentration to NO_x concentration in an isoprene-dominated forested environment (Fig. 1B).

RESULTS

The median and interquartile ranges of measured C_{ISOP} and C_{PROD} are plotted by hour in Fig. 2 (A and B). The dry and wet season data sets are represented by red and blue colors, respectively. The product concentration C_{PROD} represents the sum concentration of methyl vinyl ketone (MVK, C_4H_6O), methacrolein (MACR; C_4H_6O), and isoprene-derived hydroperoxide isomers [including (1,2)-ISOPOOH and (4, 3)-ISOPOOH, hereafter ISOPOOH; $C_5H_{10}O_3$]. MVK and MACR are the major OH-reaction products of isoprene along NO-mediated pathways (*17*). The

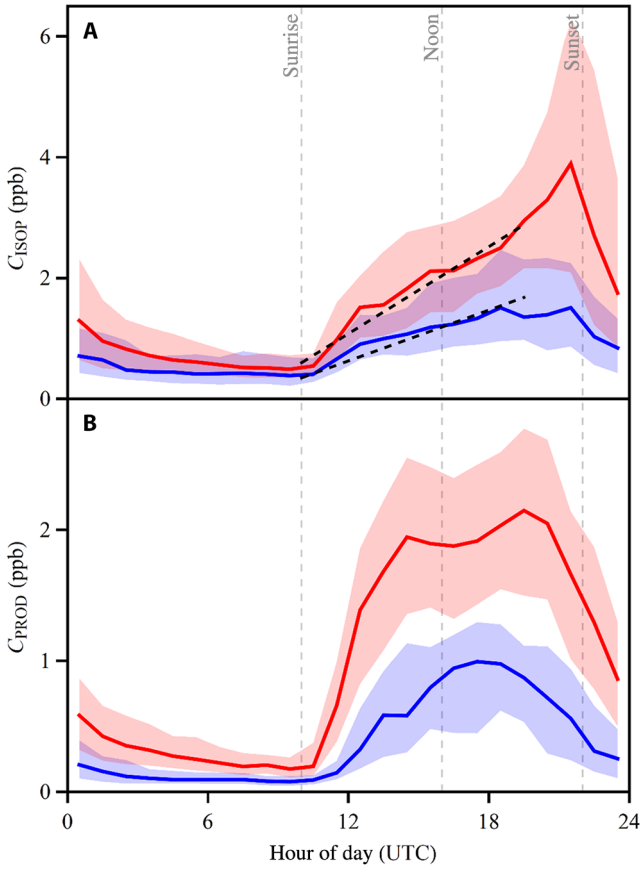

Fig. 2. Hourly variation of VOC concentrations. (**A**) Isoprene concentration C_{ISOP} and (**B**) sum concentration C_{PROD} of isoprene oxidation products. The vertical dashed gray lines demarcate local sunrise, noon, and sunset (UTC less 4 hours). Data are shown in the wet and dry seasons in blue and red colors, respectively. The solid line and shaded regions, respectively, represent the median and interquartile ranges of the data sets for each hour of the day. The two black dashed lines in (A) show the simulated increase of C_{ISOP} from sunrise to midafternoon using Eq. 2 for $C_{ISOP,0}$ values of 0.35 and 0.6 ppb.

ISOPOOH species are the major products along HO_2-mediated pathways (*30*). Although the relative importance of the NO and HO_2 pathways varies with NO_x concentration (*29*), the summed production yield of MVK, MACR, and ISOPOOH is approximately 70% across the atmospherically relevant range of NO_x concentrations (*30*).

Figure 2 (A and B) shows that before sunrise, C_{ISOP} and C_{PROD} were <20 and <10% of their respective afternoon values. At sunrise, the forest began to emit isoprene, and photochemical production of OH also began. Isoprene had a lifetime of 2.8 hours against OH attack for $C_{OH} = 1.0 \times 10^6$ cm^{-3}, whereas the lifetimes of products against chemical loss were up to five times higher. In line with these processes, Fig. 2 (A and B) shows that at sunrise, C_{ISOP} increased, followed shortly thereafter by increases in C_{PROD}. Isoprene also reacted with photochemically produced O_3, but this pathway was typically one order of magnitude less important than the OH pathway for the prevailing atmospheric conditions (*26*). The resulting MVK and MACR was a minor contribution to the overall production of these species. In addition to chemical loss and production, C_{ISOP} and C_{PROD} were also affected by dry and wet deposition, as well as by entrainment of air from above the boundary layer. The analysis herein focuses on afternoon concentrations C_{ISOP} and C_{PROD} because OH oxidation has the greatest impact on C_{ISOP} and C_{PROD} at this time of the day. In addition, the possibility of intercepting a polluted air mass from Manaus was highest in the afternoon, given that the research site was 4 to 6 hours downwind of this pollution source for typical winds following sunrise (*28*).

Scatterplots for the afternoon hours (13:00 to 16:00 local time) of C_{ISOP}, C_{PROD}, and C_{PROD}/C_{ISOP} in relation to the sum concentration C_{NO_y} of reactive nitrogen species (NO_y) are shown in Fig. 3, A to C, respectively. In addition to the NO_x species, the NO_y family also included reservoir forms of oxidized nitrogen, such as HNO_3, which were products of atmospheric reactions of NO_x (*3*). A few hours downwind of the Manaus source region at the observation site, C_{NO_y} remained a semiconserved quantity, whereas C_{NO_x} had significantly decreased. Atmospheric conversion of NO_x to NO_y also occurred for air masses downwind of regional biomass burning. Therefore, for the analysis, C_{NO_y} was used to represent the integrated intensity of NO_x chemistry before arrival of an air mass at the observation site (*29*, *31*). The ratio C_{NO_x}/C_{NO_y} had an interquartile variability of 0.30 to 0.44 across the study period, supporting the use of the simplified representation C_{NO_y}. As shown in Fig. 3, the hourly averaged afternoon values of C_{NO_y} spanned more than one order of magnitude from 0.3 to 3.5 parts per billion (ppb). The interquartile range of C_{NO_y} in the afternoon hours was 0.7 to 1.2 ppb in the wet season and 1.3 to 2.0 ppb in the dry season. As a reference point, C_{NO_y} for regional background conditions was 0.46 ± 0.26 ppb (*32*). Concentrations above 1 ppb at the observation site indicated the effects of Manaus pollution or regional biomass burning (*29*, *31*).

The scatterplots of Fig. 3 illustrate the following findings. C_{ISOP} did not correlate with C_{NO_y} (Spearman's rank $P = 0.4$ and correlation coefficient $r = -0.07$; Fig. 3A). C_{PROD} did correlate with C_{NO_y} ($P < 10^{-4}$; Fig. 3B), yet the data were scattered ($r = 0.4$). By comparison, the ratio C_{PROD}/C_{ISOP} correlated tightly with C_{NO_y} ($P < 10^{-4}$ and $r = 0.6$; Fig. 3C). The median of C_{PROD}/C_{ISOP} increased from 0.4 to 1.0 as C_{NO_y} changed from below 0.5 to above 2 ppb. A high value of C_{PROD}/C_{ISOP} was never observed for a low value of C_{NO_y} (Fig. 3C).

An unclear trend in the concentration plots on the one hand (Fig. 3, A and B) compared to a clear trend in the ratio plot on the other hand (Fig. 3C) with respect to C_{NO_y} can be explained by the large temporal variability in isoprene emissions (*22*). This variability was independent

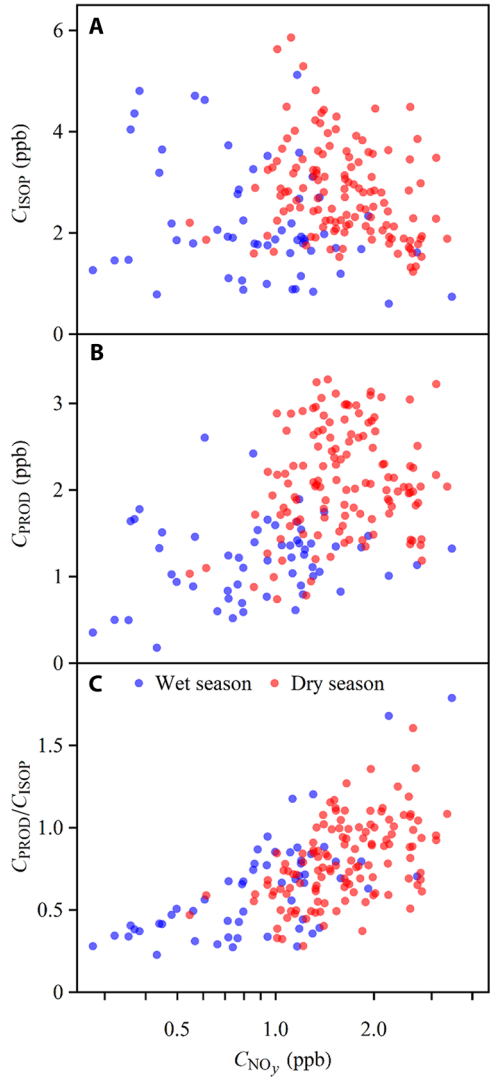

Fig. 3. Scatterplots of VOC concentrations with NO_y concentration. (**A**) Isoprene concentration C_{ISOP}. (**B**) Sum concentration C_{PROD} of isoprene oxidation products. (**C**) Concentration ratio C_{PROD}/C_{ISOP}. Data points represent hourly averages recorded within a time window of 13:00 to 16:00 (local time) (17:00 to 20:00 UTC). Blue and red points correspond to the wet and dry seasons, respectively, for fair-weather conditions. All weather data, including periods of heavy rainfall or prolonged overcast conditions, are presented in fig. S1.

of C_{NO_y} and, thus, confounded direct relationships between C_{ISOP} and C_{NO_y} or C_{PROD} and C_{NO_y}. By comparison, the ratio C_{PROD}/C_{ISOP} largely compensated the variability in isoprene emissions and thereby revealed differences in atmospheric oxidation. For these reasons, C_{PROD}/C_{ISOP} was used in the further analysis herein, focusing on understanding and quantifying the effects of pollution on the atmospheric oxidation cycle over central Amazonia.

DISCUSSION

Relating OH concentration to the ratio C_{PROD}/C_{ISOP}

A model of isoprene photochemistry over the course of 1 day was constrained by the observed values of C_{PROD}/C_{ISOP} to estimate the equivalent noontime OH concentration for the preceding daytime

hours upwind of the observation site, as follows. For products species i of isoprene oxidation, where i is one of (1,2)-ISOPOOH, (4,3)-ISOPOOH, MVK, or MACR, the time course of product concentrations $C_i(t)$ in an air mass is governed by the following family of equations

$$\frac{dC_i}{dt} = y_i(\mathrm{NO})\ k_{\mathrm{ISOP,OH}}\ C_{\mathrm{OH}}(t)\ C_{\mathrm{ISOP}}(t) + y_{i,\mathrm{O_3}}\, k_{\mathrm{ISOP,O_3}} C_{\mathrm{O_3}}(t)\ C_{\mathrm{ISOP}}(t) - k_i(t)\ C_i(t) \quad (1)$$

where y_i is the production yield of product species i from the reaction between hydroxy radical and isoprene. It varies according to the fate of ISOPOO, which is largely controlled by the NO concentration and hence susceptible to pollution. $C_{\mathrm{OH}}(t)$, $C_{\mathrm{ISOP}}(t)$, and $C_{\mathrm{O_3}}(t)$, where t represents time, are the concentrations of hydroxyl radical, isoprene, and ozone, respectively, all of which vary strongly with time of day. $k_{\mathrm{ISOP,OH}}$ and $k_{\mathrm{ISOP,O_3}}$ are the reaction rate constants of isoprene with hydroxyl radical and ozone, respectively. $y_{i,\mathrm{O_3}}$ is the production yield of product species i from the reaction between ozone and isoprene (*30*). k_i is a composite, pseudo–first-order loss coefficient of species i, given by $k_i(t) = k_{i,\mathrm{OH}}\, C_{\mathrm{OH}}(t) + k_{i,\mathrm{O_3}}\, C_{\mathrm{O_3}}(t) + k_{i,\mathrm{en}} + k_{i,\mathrm{de}}$ for bimolecular reaction between species i and OH or O_3, entrainment mixing with air above the boundary layer (en), and deposition to the planetary surface (de). Table S1 lists values of $y_{i,\mathrm{O3}}$, $k_{i,\mathrm{OH}}$, and $k_{i,\mathrm{O3}}$, as well as typical values of $k_{i,\mathrm{en}}$ and $k_{i,\mathrm{de}}$ for central Amazonia, partly reproduced from Liu *et al.* (*29*). For comparison, a more detailed model for entrainment to couple chemistry and boundary layer dynamics was also explored, and similar results were obtained (see the Supplementary Materials).

The text below first discusses the sequential reaction model (SRM), which is a commonly used simplification of Eq. 1 to relate an observed ratio $C_{\mathrm{PROD}}/C_{\mathrm{ISOP}}$ to an inferred OH concentration (*21*). The conclusion reached is that the SRM is not appropriate for analysis of the collected data set. The text then introduces a complementary approach based on (i) time-dependent approximations of C_{ISOP}, C_{OH}, and $C_{\mathrm{O_3}}$ and (ii) substitution of the production yield $y_i(\mathrm{NO})$ by an effective production yield denoted by $y_i^*(C_{\mathrm{NO}_y})$.

Analysis by SRM assumes that isoprene emissions can be taken as a point source (typically an upwind forest) and that isoprene is subsequently oxidized during transport to an observation site. More specifically, isoprene is not emitted into the air parcel along its path of travel, and reaction with OH is the dominant process governing the time evolution of C_{ISOP} (that is, $dC_{\mathrm{ISOP}}/dt = -k_{\mathrm{ISOP,OH}}\, C_{\mathrm{OH}}\, C_{\mathrm{ISOP}}$). Other assumptions include constant C_{OH} and $C_{\mathrm{O_3}}$, a fixed y_i, a fixed reaction time t, and negligible entrainment and deposition. For these conditions, Eq. 1 transforms to an explicit relation that allows C_{OH} to be inferred from measured $C_{\mathrm{PROD}}/C_{\mathrm{ISOP}}$ (*21*). The major underlying SRM assumption of an upwind point source was, however, not applicable to the GoAmazon2014/5 scenario. The observation site was surrounded by forest for hundreds of kilometers, meaning that isoprene was continuously emitted into air parcels throughout transport and that C_{ISOP} and C_{PROD} corresponded to the integrated balance between source and loss processes throughout transport.

An alternative scheme to the SRM is developed herein to constrain C_{OH} based on observed $C_{\mathrm{PROD}}/C_{\mathrm{ISOP}}$. The regional area around T3 is approximated as a homogeneous forest representing a perfectly diffuse nonpoint source region of isoprene. Analysis using Google Earth shows that surface forest coverage exceeded 70% in a 100-km radius for the dominating easterlies and northeasterlies in the wind rose and >80% for all directions (*33*). The radius of 100 km was based on typical wind speeds of 10 to 20 km h^{-1} and the time period from the start of photochemistry at daybreak to the analysis window in the afternoon. Within this 100-km radius, the forest type and, hence, isoprene emissions varied to some extent (*34*), and there were also scattered pastures, two large rivers, and the urban area of Manaus. These factors notwithstanding, a homogeneous diffuse source of isoprene emissions was taken as an acceptable approximation for the accuracy of the modeling herein.

Under this approach of a homogeneous source region, a time series of observations at a Eulerian point is fully transformable into a Lagrangian model of a time series of concentrations within an air parcel over the course of a time period (*35*, *36*). Equation 1 describes the transformations of product species C_i within the Lagrangian parcel, and in the treatment herein, observations constrained the terms. For instance, measurements of the time course of isoprene concentrations directly constrained $C_{\mathrm{ISOP}}(t)$. Steady increases were observed from sunrise to midafternoon (Fig. 2A), and the observed time dependence was represented empirically by the following linear equation

$$C_{\mathrm{ISOP}}(t) = \xi\ C_{\mathrm{ISOP,0}}\ (1 + t/t^*_{\mathrm{ISOP}}) \quad (2)$$

where ξ was a daily scaling factor representing the variability in isoprene concentrations for each day, $C_{\mathrm{ISOP,0}}$ was the typical isoprene concentration at time zero (sunrise), and t^*_{ISOP} was the typical characteristic time for C_{ISOP} to double its initial value. A value of 2.5 hours for t^*_{ISOP} represented most days. Values of $C_{\mathrm{ISOP,0}}$ of 0.35 and 0.6 ppb were used as approximate values to represent the wet and dry seasons, respectively. Equation 2 is plotted in Fig. 2A as the black dashed lines to represent median $C_{\mathrm{ISOP}}(t)$ from sunrise to midafternoon in the two seasons using ξ of unity. The analysis below further shows that the quantities ξ and $C_{\mathrm{ISOP,0}}$ drop out (Eq. 5) so that the actual values are not important.

In regard to $C_{\mathrm{OH}}(t)$, hydroxyl radical concentrations strongly correlate with the photolysis frequency $J_{\mathrm{O_3}}$ of ozone for most locations worldwide (*37*). In the analysis, the daily course of hydroxyl radical concentrations was approximated as an equivalent noontime concentration $C_{\mathrm{OH,noon}}$ modulated by a time-dependent photolysis frequency $J_{\mathrm{O_3}}$ of ozone along the $O(^1D)$ channel, as follows

$$C_{\mathrm{OH}}(t) = C_{\mathrm{OH,noon}} \frac{J_{\mathrm{O_3}}(t)}{J_{\mathrm{O_3,noon}}} \quad (3)$$

where $J_{\mathrm{O_3,noon}}$ was the peak value occurring at local noon for the equatorial location. The variation of $J_{\mathrm{O_3}}(t)/J_{\mathrm{O_3,noon}}$ followed that of the Master Chemical Mechanism for clear skies at the latitude and longitude of the observation site (fig. S2) (*30*). The value of $C_{\mathrm{OH,noon}}$ was not known before the analysis, and inferring its value was a main point of the analysis presented herein.

The production yield $y_i(\mathrm{NO})$ in Eq. 1, written in full form as $y_i[C_{\mathrm{NO}}(t)]$, does not fulfill the homogeneity requirement of a Eulerian-to-Lagrangian transformation because of the decreasing concentration of NO along the path. The observations and analysis presented in the study of Liu *et al.* (*29*) for this same observation site showed that the ratio of product concentrations $C_{\mathrm{ISOPOOH}}/C_{\mathrm{MVK+MACR}}$ correlated tightly with C_{NO_y}, and this ratio was further transformed in that study to the effective production ratio $y^*_{\mathrm{ISOPOOH}}/y^*_{\mathrm{MVK+MACR}}$ by combining the measurements with kinetic modeling (*29*). Herein, the production

yield $y_i[C_{NO}(t)]$ in the Lagrangian framework was substituted by an empirical effective production yield $y_i^*(C_{NO_y})$. The relationship $y_i^*(C_{NO_y})$ is presented in fig. S3 (see further in the Supplementary Materials). This treatment subsumed the reality of a detailed history of NO exposure within the sampled air parcel along its Eulerian path into an effective behavior, which was empirically quantified by semi-conserved C_{NO_y} during the course of Lagrangian time. Although this approach was approximate, the tight relationship of concentration ratio and C_{NO_y} observed in the study of Liu *et al.* (*29*) supported its use for the analysis herein.

The quantity $C_{O_3}(t)$ in Eq. 1 was directly constrained by two observations: (i) the increase of ozone concentrations from sunrise to midafternoon (fig. S4A) and (ii) the correlation between C_{O_3} and C_{NO_y} for afternoon time periods (fig. S4B). On the basis of these observations, $C_{O_3}(t)$ for an air parcel arriving at the observation site in the afternoon was empirically approximated as a function of observed C_{NO_y}. Specifically, $C_{O_3}(t)$ was represented by $C_{O_3}(C_{NO_y}, t)$, as explained further in the Supplementary Materials. Overall, sensitivity tests presented herein show that the influence of ozone chemistry on C_{PROD}/C_{ISOP} and, hence, inferred $C_{OH,noon}$ was small.

For these treatments of $C_{ISOP}(t)$, $C_{OH}(t)$, $C_{O_3}(t)$, and $y_i(NO)$, Eq. 1 can be rewritten as follows

$$\begin{cases} \dfrac{dC_i}{dt} = \left[y_i^*(C_{NO_y})\ k_{ISOP,OH}\ C_{OH,noon}\ \dfrac{J_{O_3}(t)}{J_{O_3,noon}} + \right. \\ \qquad \left. y_{i,O_3}\, k_{ISOP,O_3}\, C_{O_3}(C_{NO_y}, t) \right] C_{ISOP,0}\ \xi\ \left(1 + \dfrac{t}{t^*_{ISOP}}\right) - \\ \qquad k_i(t)\ C_i(t) \\ C_i(0) = 0 \end{cases} \quad (4)$$

The initial concentrations of product species i are taken as zero [that is, $C_i(0) = 0$] based on the data sets of Fig. 2. The symbol ς_i, defined by $\varsigma_i = C_i/C_{ISOP}$, is introduced for the product ratio. By definition, $C_{PROD}/C_{ISOP} = \Sigma_i\, \varsigma_i$. The following equation holds for $d\varsigma_i/dt$

$$\begin{cases} \dfrac{d\varsigma_i}{dt} = y_i^*(C_{NO_y})\ k_{ISOP,OH}\ C_{OH,noon}\ \dfrac{J_{O_3}(t)}{J_{O_3,noon}} + \\ \qquad y_{i,O_3}\, k_{ISOP,O_3}\, C_{O_3}(C_{NO_y}, t) - \left(k_i(t) + \dfrac{1}{t^*_{ISOP} + t}\right)\varsigma_i(t) \\ \varsigma_i(0) = 0 \end{cases} \quad (5)$$

Equation 5 is derived in the Supplementary Materials. The scaling factor ξ and the initial concentration $C_{ISOP,0}$ drop out. Equation 5 captures the behavior shown in Fig. 3 that the ratio C_{PROD}/C_{ISOP} is independent of isoprene emissions even as the product concentration C_{PROD} is not. Equation 5 also suggests that the NO_x exposure of the air mass, represented by C_{NO_y} here, is a key driver of C_{PROD}/C_{ISOP} under ambient conditions through (i) effects on $y_i^*(C_{NO_y})$, (ii) effects on $C_{O_3}(C_{NO_y})$, and (iii) possible effects on $C_{OH,noon}(C_{NO_y})$.

The relative sensitivity of the analysis to $y_i^*(C_{NO_y})$, $C_{O_3}(C_{NO_y})$, and $C_{OH,noon}(C_{NO_y})$ is examined in Fig. 4. The figure shows C_{PROD}/C_{ISOP} as a function of C_{NO_y} for two fixed values of $C_{OH,noon}$, specifically 1×10^6 and 2×10^6 cm^{-3}, using Eq. 5 with and without ozone chemistry. At fixed $C_{OH,noon}$, C_{NO_y} affects C_{PROD}/C_{ISOP} via the effects on $y_i^*(C_{NO_y})$ and $C_{O_3}(C_{NO_y})$. Figure 4 shows that a doubling in $C_{OH,noon}$ is a dominant effect on C_{PROD}/C_{ISOP} relative to the minor effects of y_i^* and C_{O_3}. Shifts due to presence or absence of ozone chemistry are less than 10%.

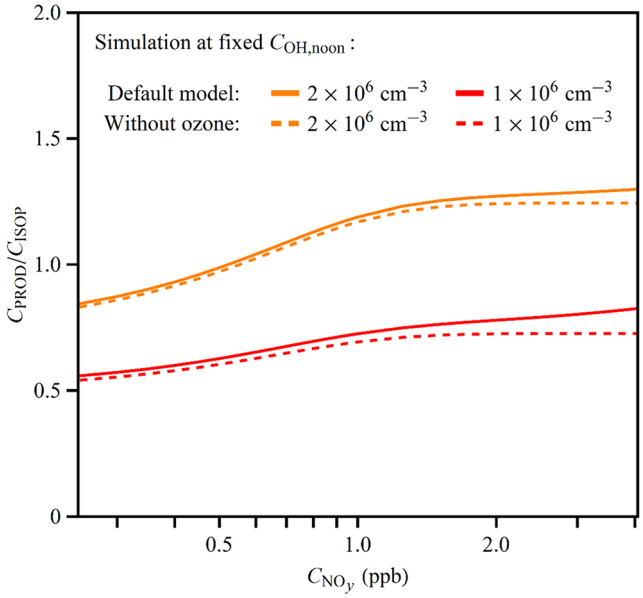

Fig. 4. Simulated dependence of the concentration ratio C_{PROD}/C_{ISOP} on NO_y concentration C_{NO_y}. Results are shown for two different values of $C_{OH,noon}$, as well as the full model compared to a model that omitted isoprene ozonolysis. At fixed $C_{OH,noon}$, C_{NO_y} affects C_{PROD}/C_{ISOP} via the effects on $y_i^*(C_{NO_y})$ and $C_{O_3}(C_{NO_y})$ (Eq. 5). Solid lines show results for the full model of Eq. 5, and dashed lines show results for a model that omits isoprene ozonolysis (that is, $C_{O_3} = 0$). For all cases, t = 8.5 hours, corresponding to 14:30 (local time).

The simulations in Fig. 4 can be compared to the observations in Fig. 3C. They are in agreement that C_{PROD}/C_{ISOP} increases for greater C_{NO_y}. For fixed $C_{OH,noon}$, the relative increase is, however, smaller in the simulation than in the observations. For an increase of C_{NO_y} from 0.3 to 3.5 ppb, the simulated increase of C_{PROD}/C_{ISOP} is 50 to 60% for fixed OH concentration, whereas the observed increase is greater than 200%. Changes in y_i^* and C_{O_3} with C_{NO_y} thus do not fully explain the observed dependence of C_{PROD}/C_{ISOP} on C_{NO_y}. The implication is that changes in $C_{OH,noon}$ with C_{NO_y} are important for explaining the observations. More specifically, $C_{OH,noon}(C_{NO_y})$ can be inferred from the data set of $C_{PROD}/C_{ISOP}(C_{NO_y})$.

To do so, Eq. 5 was used in conjunction with the data set of $C_{PROD}/C_{ISOP}(C_{NO_y})$ plotted in Fig. 3C to estimate the associated values of equivalent noontime OH concentration $C_{OH,noon}$. The values are described as equivalent, given the approximation of the diel variation of $C_{OH}(t)$, as well as the path-averaging inherent in $y_i^*(C_{NO_y})$. For this analysis, projected values of C_{PROD}/C_{ISOP} were calculated by integrating Eq. 5 and summing the resultant concentration ratio ς_i of individual products for processing times of 7.5, 8.5, and 9.5 hours across an array of atmospherically relevant values of $C_{OH,noon}$ and C_{NO_y}. A lookup matrix of four dimensions (that is, C_{PROD}/C_{ISOP}, $C_{OH,noon}$, C_{NO_y}, and t) was thereby created. A value of $C_{OH,noon}$ was obtained from the matrix based on (C_{PROD}/C_{ISOP}, C_{NO_y}, t) for each data point of Fig. 3C. The values of $C_{OH,noon}$ ranged from 0.3×10^6 to 4×10^6 cm^{-3} across the data set of Fig. 3C. The quartiles were 0.8×10^6, 1.1×10^6, and 1.4×10^6 cm^{-3}.

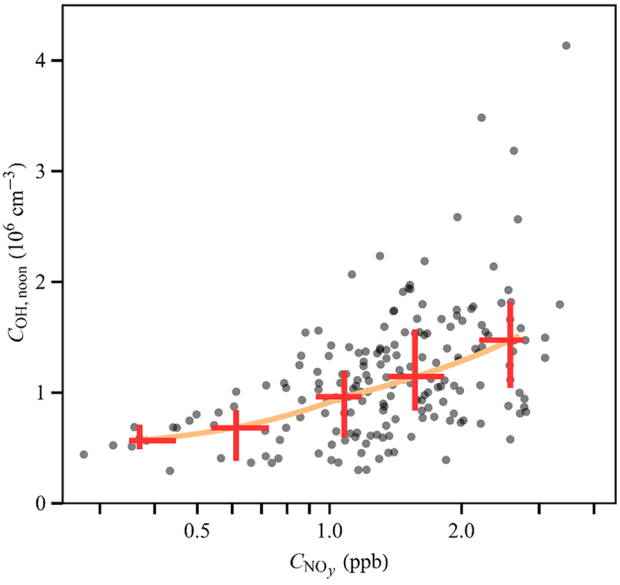

Fig. 5. Dependence of inferred equivalent noontime OH concentration $C_{OH,noon}$ on NO_y concentration. The gray dots represent $C_{OH,noon}$ inferred for the individual data points of Fig. 3C. The red crosses represent medians and quartiles after grouping the data points into five equally spaced bins based on logarithmic NO_y concentrations. The orange line connects the medians of the binned data.

The values for $C_{OH,noon}$ estimated by this analysis represent effective noontime OH concentrations that the air parcel experienced, embodying the history of oxidative capacity along its path of travel before arrival at the observation site.

Dependence of $C_{OH,noon}$ on C_{NO_y}

The retrieved $C_{OH,noon}$ values are plotted versus C_{NO_y} in Fig. 5. The data points distribute below the 45° line of the plot, indicating that high OH concentrations occurred only for high C_{NO_y}. For further statistics, the $C_{OH,noon}$ values were grouped by equally spaced logarithmic bins of C_{NO_y}, and quartile and median values were taken for each subset. The median values of $C_{OH,noon}$ increased monotonically with median values of C_{NO_y}. For the subset of lowest C_{NO_y}, corresponding to a median value of 0.4 ppb, the median value of $C_{OH,noon}$ was 0.6×10^6 cm^{-3}. For the subset of highest C_{NO_y}, corresponding to a median value of 2.6 ppb, the median value of $C_{OH,noon}$ was 1.5×10^6 cm^{-3}. The median value of $C_{OH,noon}$ thus increased by 250% for a shift in C_{NO_y} from 0.4 to 2.6 ppb.

Even as there is a clear increasing trend of $C_{OH,noon}$ for increasing C_{NO_y} (Fig. 5), there is also a scatter in the data for high C_{NO_y}. The scatter at high C_{NO_y} could be related to some underlying approximations in the retrieval of $C_{OH,noon}$, such as the use of C_{NO_y} to represent integrated NO_x exposure. The omission from the model of possible wet deposition upwind of the observation site might also be a major factor. Although the data were screened for fair weather locally, patchy afternoon precipitation, caused by locally induced thermal convection, frequently occurred in the study region (*38*). In the case that an air parcel encountered a rainfall event before arriving at the observation site, the more soluble oxidation products of isoprene might be removed preferentially relative to isoprene, and the retrieved $C_{OH,noon}$ values for these cases would be biased low. The suggestion then is that the line drawn in Fig. 5 is a lower estimate of the increase in $C_{OH,noon}$ for increasing C_{NO_y} because of omission of wet deposition in the analysis.

Entrainment of air aloft accompanying the growth of the convective boundary layer is another important process that can affect the inferred $C_{OH,noon}$ values. Sensitivity tests were performed to evaluate the treatment embedded in $k_i(t)$ of Eq. 1 as compared to a more detailed mixing model. The results, presented in the Supplementary Materials, suggest that $C_{OH,noon}$ can be underestimated on the order of 20% for higher values of C_{NO_y}, again indicating that the line drawn in Fig. 5 can be an underestimate.

Random measurement errors of C_{PROD}, C_{ISOP}, and C_{NO_y}, and systematic errors in the parameterizations of $C_{OH}(t)$, $C_{ISOP}(t)$, and $y_i^*(C_{NO_y})$ were also considered. The methods are presented in the Supplementary Materials (see table S2). As a result, inferred $C_{OH,noon}$ values are estimated to have a standard error of ±30%. This uncertainty is small relative to the trend of an increase by 250% of $C_{OH,noon}$ from small to high C_{NO_y}.

In the context of the controversy involving direct OH observations (*9*, *19*, *20*), the inference of OH concentrations from measurements of isoprene and its oxidation products, as presented herein, represents an important, albeit indirect, complementary analysis. The result presented in Fig. 5 serves as counterevidence to the conclusion of the earlier meta-study, suggesting that OH concentrations are independent of NO_x in low-NO_x, high-isoprene environments (*4*). The OH concentrations obtained herein were 80% lower than those reported using the LIF technique over rainforest in coastal eastern South America for similar isoprene concentrations. By comparison, the OH concentrations inferred by the analysis herein were comparable to concurrent GoAmazon2014/5 observations using chemical ionization mass spectrometry deployed at the same observation site (see the Supplementary Materials). In addition, the OH concentrations fell into the range of OH concentrations inferred from previous airborne measurements over tropical forests in South America (see table S3 and references therein).

In summary, the current study shows that OH concentrations inferred from measurements of isoprene and its oxidation products increased with increasing NO_y concentrations over a tropical forest in the central Amazon basin, in support of the bell curve response represented in Fig. 1. This result suggests that the oxidation capacity over tropical forests is susceptible to anthropogenic NO_x emissions. Looking into the future in Amazonia, trends of ongoing deforestation for agricultural purposes and expanding urbanization can be expected to increase demand for electricity and transport (*39*). Increased NO_x emissions should be expected on the basis of current technologies. Hydroxyl radical concentrations can be expected to likewise increase, keeping other factors equal, in forested regions affected by anthropogenic pollution in Amazonia. Increased OH concentrations imply changed spatial and temporal oxidation patterns for VOCs emitted from the forest, which can have follow-on effects on visibility, cloud formation, and rainfall based on shifted mass concentration, size distribution, and chemical composition of organic particulate matter (*28*, *40*).

MATERIALS AND METHODS

Measurements were made at the "T3" site of the GoAmazon2014/5 Experiment (*27*). The T3 site was located in a pasture area of 2.5 km × 2 km in central Amazonia (−3.2133°, −60.5987°). Pasture regions have low emissions of isoprene (*25*). The site was 70 km west of Manaus, Brazil. Steady equatorial trade winds passed over Manaus in the direction of T3. The region between the city and T3 was largely forested with interspersed agricultural activities, and the isoprene observed at T3 originated from the upwind forest. Depending on variability in the winds,

the fetch of air at T3 varied from background conditions of the tropical forest (that is, low NO_x) to polluted conditions under the influence of Manaus and regional biomass burning (that is, higher NO_x). Measurements were made during two intensive operating periods that took place in the wet season (01 February 2014 to 31 March 2014; IOP1) and in the dry season (15 August 2014 to 15 October 2014; IOP2).

A proton-transfer-reaction time-of-flight mass spectrometer (PTR-TOF-MS; Ionicon Analytik GmbH) was used to measure isoprene and its oxidation products (*29*). The PTR-TOF-MS was part of the Mobile Aerosol Observing System (MAOS) of the U.S. Department of Energy (DOE) (*27*). Isoprene (C_5H_8) was detected as the $C_5H_9^+$ ion. MVK (C_4H_6O), MACR (C_4H_6O), and two major isoprene-derived hydroperoxide isomers, (1,2)-ISOPOOH and (4,3)-ISOPOOH ($C_5H_{10}O_3$), were collectively detected as the $C_4H_7O^+$ ion (*29*). The instrument response was calibrated using authentic standards of these compounds. The product analysis herein was based on the sum concentration of MVK, MACR, and the two ISOPOOH isomers.

Instrumentation for measuring concentrations of reactive nitrogen oxides (NO_y) was part of MAOS. The NO_y data sets were obtained from the Atmospheric Radiation Measurement (ARM) data archive (*27*). The operational detection limit of NO_y was 0.1 ppb. The NO_y concentrations were smoothed by applying a 30-min median filter to minimize the contribution of any local transient emissions, such as vehicles. Other complementary measurements at the site, such as meteorological parameters, were also obtained through the ARM data archive (*27*).

SUPPLEMENTARY MATERIALS

Supplementary material for this article is available at http://advances.sciencemag.org/cgi/content/full/4/4/eaar2547/DC1

section S1. Use of observed C_{NO_y} to represent the average NO_x exposure
section S2. Determining relation $y_i^*(C_{NO_y})$
section S3. Approximation of C_{O_3}
section S4. Derivation of Eq. 5 in the main text
section S5. Additional note of Fig. 4 in the main text
section S6. Sensitivity tests regarding entrainment process
section S7. Error analysis
section S8. Comparison of $C_{OH,noon}$ obtained in this study with other OH studies
fig. S1. Scatterplots of VOC concentrations with NO_y concentration for all-weather condition.
fig. S2. Simulated daily variation of photolysis frequency of ozone J_{O_3}, normalized to the noontime value $J_{O_3,noon}$, based on Master Chemical Mechanism.
fig. S3. Simulated NO_y dependence of effective production yields.
fig. S4. Observation and simulation of ozone concentration C_{O_3}.
fig. S5. Simulation using a mixed boundary layer model.
fig. S6. Simulated relationship of equivalent noontime OH concentration $C_{OH,noon}$ and concentration ratio C_{PROD}/C_{ISOP} using the base-case model and a mixed boundary-layer model.
fig. S7. Variation in model parametrizations for error analysis.
table S1. Production yields and loss rate coefficients for isoprene oxidation products used in the model.
table S2. Uncertainty estimates for inferred $C_{OH,noon}$ via error propagation.
table S3. Summary of inferred OH concentrations over tropical forests in South America.
References (*41*–*50*)

REFERENCES AND NOTES

1. H. Levy II, Normal atmosphere: Large radical and formaldehyde concentrations predicted. *Science* **173**, 141–143 (1971).
2. D. H. Ehhalt, Photooxidation of trace gases in the troposphere Plenary Lecture. *Phys. Chem. Chem. Phys.* **1**, 5401–5408 (1999).
3. L. C. Valin, A. R. Russell, R. C. Cohen, Variations of OH radical in an urban plume inferred from NO_2 column measurements. *Geophys. Res. Lett.* **40**, 1856–1860 (2013).
4. F. Rohrer, K. Lu, A. Hofzumahaus, B. Bohn, T. Brauers, C.-C. Chang, H. Fuchs, R. Haseler, F. Holland, M. Hu, K. Kita, Y. Kondo, X. Li, S. Lou, A. Oebel, M. Shao, L. Zeng, T. Zhu, Y. Zhang, A. Wahner, Maximum efficiency in the hydroxyl-radical-based self-cleansing of the troposphere. *Nat. Geosci.* **7**, 559–563 (2014).
5. J. Lelieveld, T. M. Butler, J. N. Crowley, T. J. Dillon, H. Fischer, L. Ganzeveld, H. Harder, M. G. Lawrence, M. Martinez, D. Taraborrelli, J. Williams, Atmospheric oxidation capacity sustained by a tropical forest. *Nature* **452**, 737–740 (2008).
6. L. K. Whalley, P. M. Edwards, K. L. Furneaux, A. Goddard, T. Ingham, M. J. Evans, D. Stone, J. R. Hopkins, C. E. Jones, A. Karunaharan, J. D. Lee, A. C. Lewis, P. S. Monks, S. J. Moller, D. E. Heard, Quantifying the magnitude of a missing hydroxyl radical source in a tropical rainforest. *Atmos. Chem. Phys.* **11**, 7223–7233 (2011).
7. A. Hofzumahaus, F. Rohrer, K. Lu, B. Bohn, T. Brauers, C.-C. Chang, H. Fuchs, F. Holland, K. Kita, Y. Kondo, X. Li, S. R. Lou, M. Shao, L. M. Zeng, A. Wahner, Y. H. Zhang, Amplified trace gas removal in the troposphere. *Science* **324**, 1702–1704 (2009).
8. D. Tan, I. Faloona, J. B. Simpas, W. Brune, P. B. Shepson, T. L. Couch, A. L. Sumner, M. A. Carroll, T. Thornberry, E. Apel, D. Riemer, W. Stockwell, HO_x budgets in a deciduous forest: Results from the PROPHET summer 1998 campaign. *J. Geophys. Res.* **106**, 24407–24427 (2001).
9. J. Mao, X. Ren, L. Zhang, D. M. Van Duin, R. C. Cohen, J.-H. Park, A. H. Goldstein, F. Paulot, M. R. Beaver, J. D. Crounse, P. O. Wennberg, J. P. DiGangi, S. B. Henry, F. N. Keutsch, C. Park, G. W. Schade, G. M. Wolfe, J. A. Thornton, W. H. Brune, Insights into hydroxyl measurements and atmospheric oxidation in a California forest. *Atmos. Chem. Phys.* **12**, 8009–8020 (2012).
10. S. Dusanter, D. Vimal, P. S. Stevens, R. Volkamer, L. T. Molina, A. Baker, S. Meinardi, D. Blake, P. Sheehy, A. Merten, R. Zhang, J. Zheng, E. C. Fortner, W. Junkermann, M. Dubey, T. Rahn, B. Eichinger, P. Lewandowski, J. Prueger, H. Holder, Measurements of OH and HO_2 concentrations during the MCMA-2006 field campaign—Part 2: Model comparison and radical budget. *Atmos. Chem. Phys.* **9**, 6655–6675 (2009).
11. Y. Kanaya, R. Cao, H. Akimoto, M. Fukuda, Y. Komazaki, Y. Yokouchi, M. Koike, H. Tanimoto, N. Takegawa, Y. Kondo, Urban photochemistry in central Tokyo: 1. Observed and modeled OH and HO_2 radical concentrations during the winter and summer of 2004. *J. Geophys. Res. Atmos.* **112**, D21312 (2007).
12. X. Ren, H. Harder, M. Martinez, R. L. Lesher, A. Oliger, J. B. Simpas, W. H. Brune, J. J. Schwab, K. L. Demerjian, Y. He, X. Zhou, H. Gao, OH and HO_2 chemistry in the urban atmosphere of New York City. *Atmos. Environ.* **37**, 3639–3651 (2003).
13. K. D. Lu, A. Hofzumahaus, F. Holland, B. Bohn, T. Brauers, H. Fuchs, M. Hu, R. Häseler, K. Kita, Y. Kondo, X. Li, S. R. Lou, A. Oebel, M. Shao, L. M. Zeng, A. Wahner, T. Zhu, Y. H. Zhang, F. Rohrer, Missing OH source in a suburban environment near Beijing: Observed and modelled OH and HO_2 concentrations in summer 2006. *Atmos. Chem. Phys.* **13**, 1057–1080 (2013).
14. T. J. Dillon, J. N. Crowley, Direct detection of OH formation in the reactions of HO_2 with $CH_3C(O)O_2$ and other substituted peroxy radicals. *Atmos. Chem. Phys.* **8**, 4877–4889 (2008).
15. H. Fuchs, A. Hofzumahaus, F. Rohrer, B. Bohn, T. Brauers, H.-P. Dorn, R. Häseler, F. Holland, M. Kaminski, X. Li, K. Lu, S. Nehr, R. Tillmann, R. Wegener, A. Wahner, Experimental evidence for efficient hydroxyl radical regeneration in isoprene oxidation. *Nat. Geosci.* **6**, 1023–1026 (2013).
16. J. Peeters, T. L. Nguyen, L. Vereecken, HO_x radical regeneration in the oxidation of isoprene. *Phys. Chem. Chem. Phys.* **11**, 5935–5939 (2009).
17. Y. J. Liu, I. Herdlinger-Blatt, K. A. McKinney, S. T. Martin, Production of methyl vinyl ketone and methacrolein via the hydroperoxyl pathway of isoprene oxidation. *Atmos. Chem. Phys.* **13**, 5715–5730 (2013).
18. J. D. Crounse, F. Paulot, H. G. Kjaergaard, P. O. Wennberg, Peroxy radical isomerization in the oxidation of isoprene. *Phys. Chem. Chem. Phys.* **13**, 13607–13613 (2011).
19. P. A. Feiner, W. H. Brune, D. O. Miller, L. Zhang, R. C. Cohen, P. S. Romer, A. H. Goldstein, F. N. Keutsch, K. M. Skog, P. O. Wennberg, T. B. Nguyen, A. P. Teng, J. DeGouw, A. Koss, R. J. Wild, S. S. Brown, A. Guenther, E. Edgerton, K. Baumann, J. L. Fry, Testing atmospheric oxidation in an Alabama forest. *J. Atmos. Sci.* **73**, 4699–4710 (2016).
20. A. Novelli, K. Hens, C. Tatum Ernest, D. Kubistin, E. Regelin, T. Elste, C. Plass-Dülmer, M. Martinez, J. Lelieveld, H. Harder, Characterisation of an inlet pre-injector laser-induced fluorescence instrument for the measurement of atmospheric hydroxyl radicals. *Atmos. Meas. Tech.* **7**, 3413–3430 (2014).
21. C. A. Stroud, J. M. Roberts, P. D. Goldan, W. C. Kuster, P. C. Murphy, E. J. Williams, D. Hereid, D. Parrish, D. Sueper, M. Trainer, F. C. Fehsenfeld, E. C. Apel, D. Riemer, B. Wert, B. Henry, A. Fried, M. Martinez-Harder, H. Harder, W. H. Brune, G. Li, H. Xie, V. L. Young, Isoprene and its oxidation products, methacrolein and methylvinyl ketone, at an urban forested site during the 1999 Southern Oxidants Study. *J. Geophys. Res.* **106**, 8035–8046 (2001).
22. U. Kuhn, M. O. Andreae, C. Ammann, A. C. Araújo, E. Brancaleoni, P. Ciccioli, T. Dindorf, M. Frattoni, L. V Gatti, L. Ganzeveld, B. Kruijt, J. Lelieveld, J. Lloyd, F. X. Meixner, A. D. Nobre, U. Pöschl, C. Spirig, P. Stefani, A. Thielmann, R. Valentini, J. Kesselmeier, Isoprene and monoterpene fluxes from Central Amazonian rainforest inferred from tower-based and airborne measurements, and implications on the atmospheric chemistry and the local carbon budget. *Atmos. Chem. Phys.* **7**, 2855–2879 (2007).
23. T. Karl, A. Guenther, R. J. Yokelson, J. Greenberg, M. Potosnak, D. R. Blake, P. Artaxo, The tropical forest and fire emissions experiment: Emission, chemistry, and transport of biogenic volatile organic compounds in the lower atmosphere over Amazonia. *J. Geophys. Res. Atmos.* **112**, D18302 (2007).

24. R. G. Prinn, R. F. Weiss, B. R. Miller, J. Huang, F. N. Alyea, D. M. Cunnold, P. J. Fraser, D. E. Hartley, P. G. Simmonds, Atmospheric trends and lifetime of CH_3CCl_3 and global OH concentrations. *Science* **269**, 187–192 (1995).
25. A. B. Guenther, X. Jiang, C. L. Heald, T. Sakulyanontvittaya, T. Duhl, L. K. Emmons, X. Wang, The model of emissions of gases and aerosols from nature version 2.1 (MEGAN2.1): An extended and updated framework for modeling biogenic emissions. *Geosci. Model Dev.* **5**, 1471–1492 (2012).
26. R. Atkinson, J. Arey, Gas-phase tropospheric chemistry of biogenic volatile organic compounds: A review. *Atmos. Environ.* **37**, 197–219 (2003).
27. S. T. Martin, P. Artaxo, L. A. T. Machado, A. O. Manzi, R. A. F. Souza, C. Schumacher, J. Wang, M. O. Andreae, H. M. J. Barbosa, J. Fan, G. Fisch, A. H. Goldstein, A. Guenther, J. L. Jimenez, U. Pöschl, M. A. Silva Dias, J. N. Smith, M. Wendisch, Introduction: Observations and modeling of the Green Ocean Amazon (GoAmazon2014/5). *Atmos. Chem. Phys.* **16**, 4785–4797 (2016).
28. S. T. Martin, P. Artaxo, L. Machado, A. O. Manzi, R. A. F. Souza, C. Schumacher, J. Wang, T. Biscaro, J. Brito, A. Calheiros, K. Jardine, A. Medeiros, B. Portela, S. S. de Sá, K. Adachi, A. C. Aiken, R. Albrecht, L. Alexander, M. O. Andreae, H. M. J. Barbosa, P. Buseck, D. Chand, J. M. Comstmstmstock, D. A. Day, M. Dubey, J. Fan, J. Faststt, G. Fisch, E. Fortner, S. Giangrande, M. Gilllles, A. H. Goldststein, A. Guenther, J. Hubbbbe, M. Jensen, J. L. Jimenez, F. N. Keutstsch, S. Kim, C. Kuang, A. Laskskin, K. McKinney, F. Mei, M. Millller, R. Nascimento, T. Pauliquevis, M. Pekour, J. Peres, T. Petäjä, C. Pöhlklker, U. Pöschl, L. Rizzo, B. Schmid, J. E. Shilllling, M. A. Silva Dias, J. N. Smith, J. M. Tomlmlinson, J. Tóta, M. Wendisch, The Green Ocean Amazon experiment (GoAmazon2014/5) observes pollution affecting gases, aerosols, clouds, and rainfall over the rain forest. *Bull. Am. Meteorol. Soc.* **98**, 981–997 (2016).
29. Y. Liu, J. Brito, M. R. Dorris, J. C. Rivera-Rios, R. Seco, K. H. Bates, P. Artaxo, S. Duvoisin, F. N. Keutsch, S. Kim, A. H. Goldstein, A. B. Guenther, A. O. Manzi, R. A. F. Souza, S. R. Springston, T. B. Watson, K. A. McKinney, S. T. Martin, Isoprene photochemistry over the Amazon rainforest. *Proc. Natl. Acad. Sci. U.S.A.* **113**, 6125–6130 (2016).
30. M. E. Jenkin, J. C. Young, A. R. Rickard, The MCM v3.3.1 degradation scheme for isoprene. *Atmos. Chem. Phys.* **15**, 11433–11459 (2015).
31. S. S. de Sá, B. B. Palm, P. Campuzano-Jost, D. A. Day, M. K. Newburn, W. Hu, G. Isaacman-VanWertz, L. D. Yee, R. Thalman, J. Brito, S. Carbone, P. Artaxo, A. H. Goldstein, A. O. Manzi, R. A. F. Souza, F. Mei, J. E. Shilling, S. R. Springston, J. Wang, J. D. Surratt, M. L. Alexander, J. L. Jimenez, S. T. Martin, Influence of urban pollution on the production of organic particulate matter from isoprene epoxydiols in central Amazonia. *Atmos. Chem. Phys.* **17**, 6611–6629 (2017).
32. P. S. Bakwin, S. C. Wofsy, S.-M. Fan, Measurements of reactive nitrogen oxides (NO_y) within and above a tropical forest canopy in the wet season. *J. Geophys. Res. Atmos.* **95**, 16765–16772 (1990).
33. P. Ploton, R. Pélissier, C. Proisy, T. Flavenot, N. Barbier, S. N. Rai, P. Couteron, Assessing aboveground tropical forest biomass using Google Earth canopy images. *Ecol. Appl.* **22**, 993–1003 (2012).
34. D. Gu, A. B. Guenther, J. E. Shilling, H. Yu, M. Huang, C. Zhao, Q. Yang, S. T. Martin, P. Artaxo, S. Kim, R. Seco, T. Stavrakou, K. M. Longo, J. Tóta, R. A. F. de Souza, O. Vega, Y. Liu, M. Shrivastava, E. G. Alves, F. C. Santos, G. Leng, Z. Hu, Airborne observations reveal elevational gradient in tropical forest isoprene emissions. *Nat. Commun.* **8**, 15541 (2017).
35. A. S. Monin, The structure of atmospheric turbulence. *Theory Probab. Appl.* **3**, 266–296 (1958).
36. A. J. Huisman, J. R. Hottle, M. M. Galloway, J. P. DiGangi, K. L. Coens, W. Choi, I. C. Faloona, J. B. Gilman, W. C. Kuster, J. de Gouw, N. C. Bouvier-Brown, A. H. Goldstein, B. W. LaFranchi, R. C. Cohen, G. M. Wolfe, J. A. Thornton, K. S. Docherty, D. K. Farmer, M. J. Cubison, J. L. Jimenez, J. Mao, W. H. Brune, F. N. Keutsch, Photochemical modeling of glyoxal at a rural site: Observations and analysis from BEARPEX 2007. *Atmos. Chem. Phys.* **11**, 8883–8897 (2011).
37. F. Rohrer, H. Berresheim, Strong correlation between levels of tropospheric hydroxyl radicals and solar ultraviolet radiation. *Nature* **442**, 184–187 (2006).
38. A. K. Betts, J. D. Fuentes, M. Garstang, J. H. Ball, Surface diurnal cycle and boundary layer structure over Rondônia during the rainy season. *J. Geophys. Res. Atmos.* **107**, 8065 (2002).
39. E. A. Davidson, A. C. de Araújo, P. Artaxo, J. K. Balch, I. F. Brown, M. M. C. Bustamante, M. T. Coe, R. S. DeFries, M. Keller, M. Longo, J. W. Munger, W. Schroeder, B. S. Soares-Filho, C. M. Souza, S. C. Wofsy, The Amazon basin in transition. *Nature* **481**, 321–328 (2012).
40. U. Pöschl, S. T. Martin, B. Sinha, Q. Chen, S. S. Gunthe, J. A. Huffman, S. Borrmann, D. K. Farmer, R. M. Garland, G. Helas, J. L. Jimenez, S. M. King, A. Manzi, E. Mikhailov, T. Pauliquevis, M. D. Petters, A. J. Prenni, P. Roldin, D. Rose, J. Schneider, H. Su, S. R. Zorn, P. Artaxo, M. O. Andreae, Rainforest aerosols as biogenic nuclei of clouds and precipitation in the Amazon. *Science* **329**, 1513–1516 (2010).
41. M. Trainer, D. D. Parrish, M. P. Buhr, R. B. Norton, F. C. Fehsenfeld, K. G. Anlauf, J. W. Bottenheim, Y. Z. Tang, H. A. Wiebe, J. M. Roberts, R. L. Tanner, L. Newman, V. C. Bowersox, J. F. Meagher, K. J. Olszyna, M. O. Rodgers, T. Wang, H. Berresheim, K. L. Demerjian, U. K. Roychowdhury, Correlation of ozone with NO_y in photochemically aged air. *J. Geophys. Res. Atmos.* **98**, 2917–2925 (1993).
42. J. Vilà-Guerau de Arellano, E. G. Patton, T. Karl, K. van den Dries, M. C. Barth, J. J. Orlando, The role of boundary layer dynamics on the diurnal evolution of isoprene and the hydroxyl radical over tropical forests. *J. Geophys. Res. Atmos.* **116**, D07304 (2011).
43. J. Vilà-Guerau de Arellano, K. van den Dries, D. Pino, On inferring isoprene emission surface flux from atmospheric boundary layer concentration measurements. *Atmos. Chem. Phys.* **9**, 3629–3640 (2009).
44. S. Kim, G. M. Wolfe, L. Mauldin, C. Cantrell, A. Guenther, T. Karl, A. Turnipseed, J. Greenberg, S. R. Hall, K. Ullmann, E. Apel, R. Hornbrook, Y. Kajii, Y. Nakashima, F. N. Keutsch, J. P. DiGangi, S. B. Henry, L. Kaser, R. Schnitzhofer, M. Graus, A. Hansel, W. Zheng, F. F. Flocke, Evaluation of HO_x sources and cycling using measurement-constrained model calculations in a 2-methyl-3-butene-2-ol (MBO) and monoterpene (MT) dominated ecosystem. *Atmos. Chem. Phys.* **13**, 2031–2044 (2013).
45. D. J. Jacob, S. C. Wofsy, Budgets of reactive nitrogen, hydrocarbons, and ozone over the Amazon forest during the wet season. *J. Geophys. Res. Atmos.* **95**, 16737–16754 (1990).
46. C. Warneke, R. Holzinger, A. Hansel, A. Jordan, W. Lindinger, U. Poschl, J. Williams, P. Hoor, H. Fischer, P. J. Crutzen, H. A. Scheeren, J. Lelieveld, Isoprene and its oxidation products methyl vinyl ketone, methacrolein, and isoprene related peroxides measured online over the tropical rain forest of Surinam in March 1998. *J. Atmos. Chem.* **38**, 167–185 (2001).
47. J. Williams, U. Poschl, P. J. Crutzen, A. Hansel, R. Holzinger, C. Warneke, W. Lindinger, J. Lelieveld, An atmospheric chemistry interpretation of mass scans obtained from a proton transfer mass spectrometer flown over the tropical rainforest of Surinam. *J. Atmos. Chem.* **38**, 133–166 (2001).
48. R. Atkinson, D. L. Baulch, R. A. Cox, J. N. Crowley, R. F. Hampson, R. G. Hynes, M. E. Jenkin, M. J. Rossi, J. Troe, Evaluated kinetic and photochemical data for atmospheric chemistry: Volume II—Gas phase reactions of organic species. *Atmos. Chem. Phys.* **6**, 3625–4055 (2006).
49. J. M. St. Clair, J. C. Rivera-Rios, J. D. Crounse, H. C. Knap, K. H. Bates, A. P. Teng, S. Jørgensen, H. G. Kjaergaard, F. N. Keutsch, P. O. Wennberg, Kinetics and products of the reaction of the first-generation isoprene hydroxy hydroperoxide (ISOPOOH) with OH. *J. Phys. Chem. A* **120**, 1441–1451 (2016).
50. T. B. Nguyen, J. D. Crounse, A. P. Teng, J. M. St. Clair, F. Paulot, G. M. Wolfe, P. O. Wennberg, Rapid deposition of oxidized biogenic compounds to a temperate forest. *Proc. Natl. Acad. Sci. U.S.A.* **112**, E392–E401 (2015).

Acknowledgments: Institutional support was provided by the Central Office of the Large-Scale Biosphere-Atmosphere Experiment in Amazonia, the National Institute of Amazonian Research, and Amazonas State University. We acknowledge the ARM Climate Research Facility, a user facility of the DOE, Office of Science, sponsored by the Office of Biological and Environmental Research, and support from the Atmospheric System Research program of that office. We thank Y. Li for helpful discussion on error analysis. The research was conducted under scientific license 001030/2012-4 of the Brazilian National Council for Scientific and Technological Development. **Funding:** Funding was obtained from the DOE (DE-SC0011115 and DE-SC0011122), the NSF (1628491 and 1321987), the Amazonas State Research Foundation, and the São Paulo Research Foundation (2014/05014-0 and 2017/17047-0). **Author contributions:** A.B.G., A.H.G., F.N.K., P.A., R.A.F.S., K.A.M., and S.T.M. designed the research. Y.L., R.S., S.K., S.R.S., and T.B.W. performed the research. Y.L., K.A.M., and S.T.M. analyzed the data and wrote the manuscript. All the authors discussed the results, reviewed, and commented the paper. **Competing interests:** The authors declare that they have no competing interests. **Data and materials availability:** All of the airborne measurement data used in the paper are available at www.arm.gov/campaigns/amf2014goamazon. Additional data related to this paper may be requested from the authors.

Submitted 18 October 2017
Accepted 21 February 2018
Published 11 April 2018
10.1126/sciadv.aar2547

Citation: Y. Liu, R. Seco, S. Kim, A. B. Guenther, A. H. Goldstein, F. N. Keutsch, S. R. Springston, T. B. Watson, P. Artaxo, R. A. F. Souza, K. A. McKinney, S. T. Martin, Isoprene photo-oxidation products quantify the effect of pollution on hydroxyl radicals over Amazonia. *Sci. Adv.* **4**, eaar2547 (2018).

Science Advances

Isoprene photo-oxidation products quantify the effect of pollution on hydroxyl radicals over Amazonia

Yingjun Liu, Roger Seco, Saewung Kim, Alex B. Guenther, Allen H. Goldstein, Frank N. Keutsch, Stephen R. Springston, Thomas B. Watson, Paulo Artaxo, Rodrigo A. F. Souza, Karena A. McKinney and Scot T. Martin

Sci Adv **4** (4), eaar2547.
DOI: 10.1126/sciadv.aar2547